THE JOURNAL OF PHYSICAL CHEMISTRY C

Article

pubs.acs.org/JPCC

Replacing the Al_2O_3 Shell on Al Particles with an Oxidizing Salt, Aluminum Iodate Hexahydrate. Part I: Reactivity

Dylan K. Smith,[†] Daniel K. Unruh,[‡] Chi-Chin Wu,[§] and Michelle L. Pantoya*[,†]

[†]Department of Mechanical Engineering, and [‡]Department of Chemistry, Texas Tech University, Lubbock, Texas 79409, United States

[§]Weapons and Materials Research Directorate, U.S. Army Research Laboratory, Aberdeen Proving Ground, Maryland 21005, United States

ABSTRACT: Improvements in the reactivity, measured in terms of flame speed, for aluminum-based energetic mixtures are increased by a factor of 2−3 by replacing the Al_2O_3 passivation layer of aluminum (Al) nanoparticles with aluminum iodate hexahydrate (AIH), an oxidizing salt. The Al−AIH nanoparticles are examined under transmission electron microscopy. An AIH passivation shell surrounding the Al core particle is a more reactive composite structure than Al_2O_3 passivation around Al which facilitates increased reaction rates with flame speeds as high as 3200 m/s. Flame speed measurements are used to show that reaction rates in AIH mixtures are determined by the AIH/Al_2O_3 ratio, oxygen balance, and β-HIO_3. Further optimization of these properties will ultimately boost significant increases in the reaction rates of the energetic materials presented in this article.

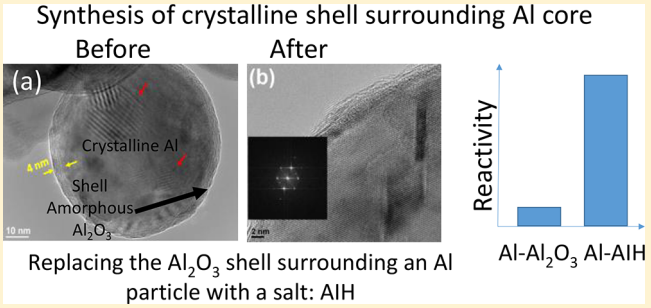

INTRODUCTION

Energetic materials contain stored chemical energy that is released upon ignition. Increasing the reaction rate of an energetic material will correspondingly increase the power delivered by the reaction. Monomolecular explosives contain relatively small levels of stored chemical energy (Figure 1) but can release that energy very quickly. These chemical reactions are triggered by kinetic mechanisms that spur bond breaking between atoms leading to fast reaction rates. Composites, on the other hand, are a mixture of fuel and oxidizer materials, discretely separated by a physical distance. These materials store a larger amount of chemical energy than monomolecular explosives (Figure 1) but are diffusion limited which inhibits the rate of energy release. Metallic fuels in composite energetic materials may have the potential to overcome limitations resulting from diffusion-based reaction mechanisms.

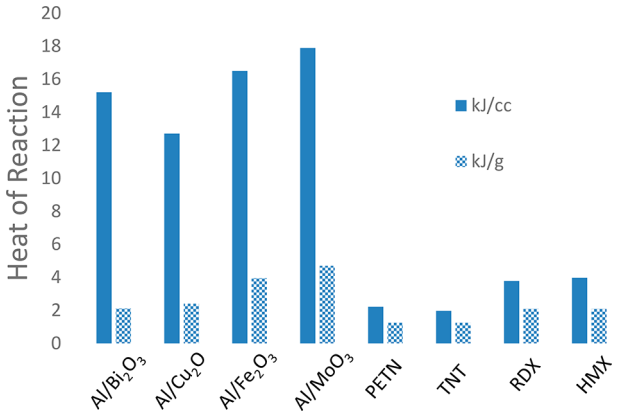

Figure 1. Heat of reaction for selected thermites and explosives.[2,3] Solid bars are in units of kJ/cc, and hatched bars are in units of kJ/g.

When metal fuels are mixed with metal oxides, the reactant mixture is commonly referred to as thermite (see example thermites in Figure 1). Mass diffusion kinetics for thermite reactions result in significant energy released relatively slowly compared with explosives.[1] For example, the heats of reaction for selected thermites and common explosives are presented in Figure 1 and show that the stored energy in thermites is significantly greater than that in explosives. However, flame speeds for thermites are generally below 1000 m/s while detonation velocities for explosives are above 7000 m/s.

Aluminum (Al) is a common fuel used in thermites due to its high energy density (16.4 kJ/g Al_2O_3)[1] when reacted with oxygen to form Al_2O_3. This reaction also happens naturally in an oxygen-containing environment producing an alumina passivation layer around unoxidized Al particles during synthesis. The passivation layer is inert and acts as a diffusion barrier and heat sink, reducing the total energy liberated and reaction rate in Al-based thermites.[4] Another limiting factor for energy release rates in composite materials is the large distance between fuel and oxidizer that is directly related to the size and shape of fuel and oxidizer particles. To decrease the limitations imposed by particle size, synthetic methods that produce

Received: June 13, 2017
Revised: September 16, 2017

DOI: 10.1021/acs.jpcc.7b05803
J. Phys. Chem. C XXXX, XXX, XXX−XXX

nanoscale Al particles have been utilized. Reduction of particle size has led to significant increases in reaction rates of thermites based on enhanced mass diffusion.[5] However, the reduced size in Al nanoparticles also results in increased concentration of Al_2O_3 limiting reaction rates in two ways: (1) Al_2O_3 is an insulator and absorbs the energy that is produced upon reaction, and (2) Al_2O_3 acts as a barrier in mass diffusion, inhibiting oxygen from reacting with unoxidized Al (Al^0) in the core of Al nanoparticles. Therefore, reducing the limiting effects of the Al_2O_3 layer can result in faster kinetics that approach those of common organic explosives.[6]

Halogenated oxidizers have been used to reduce the inhibiting effects of the Al_2O_3 passivation layer.[7] Halogens are electronegative and can react exothermically with the Al_2O_3 passivation layer in a reaction that has been coined "a pre-ignition reaction" (PIR).[4] Recently, a PIR was observed at the surface of Al particles and produced by the exothermic reaction between the alumina passivation shell encapsulating aluminum particles and iodine, specifically, iodic acid (HIO_3).[8] A relationship between flame speed and the concentration of water used during mixing of I_2O_5 and Al nanoparticles had been discovered by Smith et al.[8] The relationship is a result of the formation of aluminum iodate hexahydrate (AIH), ($Al(IO_3)_3(HIO_3)_2.6H_2O$).[9] In fact, Al−AIH mixtures exhibited increased flame speeds compared to all other Al-containing thermites with measured flame speeds as high as 3200 m/s.[9]

To begin to understand the heightened reactivity of AIH mixtures, one must examine the crystal structure of AIH. The crystal structure of AIH consists of aluminum hexahydrate ($Al(H_2O)_6^{3+}$) cations, also referred to as hexaaquoaluminum-(III),[10] held in the pore space of an iodate framework through hydrogen bonds (see Figure 1 in Smith et al.[9]). Since the oxidation state of Al in AIH is already 3+ (i.e., Al^{3+} is already oxidized), the energy released from forming Al_2O_3 from AIH is significantly less (possibly endothermic) than that from forming Al_2O_3 from Al^0. Due to Al in AIH already being oxidized (i.e., Al^{3+}), the increase in reactivity of these composite materials was not expected.[9] Therefore, the increased flame speeds seen in AIH mixtures may be a result of a kinetically driven reaction that is related to the formation of AIH. This study expands our previous work of synthesizing Al−AIH[9] nanoparticles by examining not only possible mechanisms controlling the increase in the reactivity of Al−AIH but also the crystalline structure of resultant composite nanoparticles under transmission electron microscopy (TEM). The objective is to analyze trends in reactivity as a function of AIH concentration in Al−AIH mixtures. The reactivity is assessed in terms of flame speed and reaction kinetics.

EXPERIMENTAL SECTION

Mixing Procedure. The method of mixing involves completely dissolving commercially available I_2O_5, supplied by Sigma-Aldrich (St. Louis, MO), in distilled water prior to mixing with Al nanoparticles. The commercially available I_2O_5 is comprised primarily of iodic acids[11] (i.e., HIO_3 and HI_3O_8) that dissolve in water along with I_2O_5 to form an IO_3^- solution, eliminating the need to treat the sample prior to mixing. The I_2O_5 was dissolved in a beaker with a magnetic stirrer rotating at 300 rpm in distilled water for 5 min before adding aluminum nanoparticles (~80 nm), supplied by Novacentrix (Austin, TX). Two separate reactivity studies are reported and are referred to as (1) the *water to Al ratio* study and (2) the *equivalence ratio (ER)* study. These two separate studies were designed to measure the effects of additional water concentration and initial mixing parameters on reactivity.

The water to Al ratio samples are identical to samples used in Smith et al.[9] The samples in the ER study were mixed to produce an ER value (calculated from eq 1) ranging from 0.8 to 1.5 by keeping the ratio of water to Al constant at 1:1 wt % and the ratio of water to I_2O_5 constant at 1:2.5 wt %. The 1:2.5 water to I_2O_5 ratio is the reported saturation ratio of I_2O_5 in water[12] and is the lowest concentration of water needed to dissolve I_2O_5.

Reactivity Measurements. The procedure and apparatus for measuring flame speed was previously discussed in Smith et al.[9] but will be summarized here for completeness. The liquid solutions were poured into channels milled in an acrylic plate and placed in a low-humidity (i.e., <20% relative humidity) environment to dry. The 7 cm long channels were sealed using 1 cm wide acrylic plates adhered to the top of the channel filled with sample. The purpose of the "lid" was to direct energy propagation axially along the channel. Ignition was achieved at one end of sample using a nickel−chromium wire attached to a voltage generator. The channel filled with the sample and ignition source was placed in a blast chamber with a viewing port aligned with a high-speed camera positioned perpendicular to the direction of flame propagation. Image collection was performed using a Phantom v1611 high-speed camera (Vision Research Inc.) at 381 818 frames per second (fps) and at a resolution of 384 × 64 pixels. The intensity of light created by the reaction is greatest at the leading edge of the reaction. To view this location, the f-stop on the lens (i.e., f/32) and neutral density filters were coupled to block out >99% of the light emitted to prevent oversaturation of the camera sensor. Image analysis was performed with the Phantom camera control program to monitor flame propagation and measure velocity. The time and distance measurements were exported into a spreadsheet and plotted along with a linear curve fit. All data reported produced an R^2 value greater than 0.95. Each experiment was performed in triplicate to establish repeatability.

Oxygen Ratios. For thermites, the fuel to oxygen ratio is reported as an equivalence ratio (ER), which is a ratio of the actual mass of fuel (Al^0) to mass of oxidizer over the stoichiometric mass of fuel to mass of oxidizer shown in eq 1.

$$\mathrm{ER} = \frac{\left(\frac{m_f}{m_o}\right)_{\mathrm{actual}}}{\left(\frac{m_f}{m_o}\right)_{\mathrm{stoich}}} \tag{1}$$

In eq 1, m_f is the fuel mass and m_o is the oxidizer mass. The fuel to oxidizer ratio increases as ER increases, and the stoichiometric ratio is 1.0. After mixing, the AIH crystals that formed were comprised of both Al and AIH making the determination of ER impossible assuming Al^{3+} in AIH forms Al_2O_3. Therefore, fuel to oxidizer ratio for the mixture was determined by oxygen balance (OB) shown in eq 2. Oxygen balance is calculated in terms of 100 g of compound to determine the percent of oxygen excess or deficient for 100 g of a compound.

$$\mathrm{OB\%} = \frac{-1600}{M_c} * \left(2X + \frac{Y}{2} + \alpha M - Z\right) \tag{2}$$

In eq 2, M_c is the molecular weight of the compound, X is moles of carbon (i.e., 0 for this mixture since carbon is not

DOI: 10.1021/acs.jpcc.7b05803
J. Phys. Chem. C XXXX, XXX, XXX−XXX

present), Y is moles of hydrogen, αM is moles of metallic oxide, and Z is moles of oxygen. For this mixture, Al_2O_3 is the product, so α in αM equals 1.5.

X-ray Diffraction. The samples used for powder XRD analysis are prepared identically to samples used for flame speed measurements. The data for each sample were collected on a Rigaku Ultima III powder diffractometer operated in continuous $\theta-2\theta$ mode from 15 to 60° 2θ with parallel beam geometry. The step size was 0.02° with a collection time of 2°/min. The MDI Jade V9.1.1 software provides both qualitative and quantitative data analysis used to estimate the oxygen balance of the AlH crystals formed.

Transmission Electron Microscopy. The AlH samples were further examined using TEM. The TEM specimens were prepared using high-purity ethanol as the medium via the nanoparticle suspension technique.[13] The samples were studied in a JEOL 2100FX TEM operated at 200 keV (JEOL USA, Inc.) with an emission current of approximately 120 μA. The overall field of view varied from 10 to 100 μm^2 under TEM diffraction contrast imaging conditions. All images that are shown in TEM mode are formed in the bright-field (BF) mode. The crystallinity of the sample was also examined from the fast Fourier transform (FFT) plot acquired from the corresponding TEM image. The selected aperture diffraction (SAD) pattern was obtained by inserting an aperture of appropriate size into the back focal plane of the objective lens using a 25 cm camera length. The TEM images and SAD patterns obtained from TEM were analyzed by using the Digital Micrograph microscopy software (Gatan Inc.).

RESULTS AND DISCUSSION

The reactive natures of AlH mixtures were first reported in Smith et al.,[9] and initial XRD results were presented for AlH mixtures synthesized using various water to Al ratios. Previously reported concentration data for the AlH and Al mixtures were estimates due to an unidentified phase seen in the mixtures. The unidentified phase was later determined to be the rarely reported phase β-HIO_3. Details of the synthesis and single-crystal data for β-HIO_3 were reported in Smith et al.[14] Concentration data for the various equivalence ratios (i.e., ER study) from initial mixing are tabulated in Tables 1 and 2, respectively, using quantitative XRD analyses and identification of peaks for β-HIO_3.

Table 1. Initial Mixing Concentrations

ER	Al^0 (mg)	Al_2O_3 (mg)	I_2O_5 (mg)	water (mg)
1.5	1611.2	402.8	3985	3608
1.2	1381.6	345.4	4272	3435.8
1.1	1298.4	324.6	4377	3373.8
1	1209.6	302.4	4487	3306.8
0.9	1116.8	279.2	4603	3237.2
0.8	1019.2	254.8	4725	3164

The uncertainty based on standard deviation from variation between samples and accuracy of peak fitting is shown in parentheses in Table 2. The highest uncertainty in Table 2 is less than 20% (average uncertainty less than 7%), and a similar uncertainty is assumed in all figures where calculations were performed using the data from Table 2. The data from Table 2 coupled with flame speed measurements (see Figure 2) will be used to show that the increased reactivity seen in AlH mixtures appears to be the result of AlH replacing the Al_2O_3 passivation layer around the Al particles.

Structural Analysis of Al−AlH Nanoparticles via TEM. The structures of resultant Al−AlH nanoparticles are further examined under TEM and compared with that of bare Al nanoparticles. As an example, Figure 3 shows a TEM image of a bare Al nanoparticle at 250k× magnification. Distinct lattice fringes are exhibited in the core (see red arrows in Figure 3), indicating its strong crystallinity with a conformal and amorphous oxide layer with a measured thickness of approximately 4 nm. In contrast, Figure 4 shows high crystallinity in the outer shell of both Al−AlH nanoparticles (Figure 4a and b), as exhibited by the TEM images and their corresponding FFT plots in Figure 4a and b, respectively. These particles display superior single crystallinity throughout the entire particle from the Al core to the outer AlH shell exemplified by the parallel thin straight lines corresponding to lattice spacing. In comparison to the Al particle in Figure 3, no trace of remaining amorphous Al_2O_3 layer remains in both Al−AlH particles. The AlH layer on the outer shell surrounding the Al core also conforms perfectly with the crystallinity of the Al core such that the lattice fringes appear as thin parallel straight lines and are continuous throughout the core/shell structure. This is also confirmed by the FFT plots. In Figure 4b, the FFT diffraction spots also reveal the hexagonal nature of AlH crystals with additional diffraction spots.

Figure 5 displays a SAD pattern from Al−AlH nanoparticles at a relatively low magnification of 40k×. The pattern shows discrete diffraction spots rather than amorphous rings underscoring again the single crystallinity of Al−AlH nanoparticles. As demonstrated in the figure, the majority of high-intensity diffraction spots from Al−AlH match well with the corresponding (hkl) diffraction rings of a bulk Al crystal (where the values of h, k, and l are Miller indices) outlined as green circles. Nevertheless, several dimmer diffraction spots are also visible with low intensities. The d-spacing for those extra diffraction spots that do not belong to Al is estimated to be between 0.10 to 0.25 nm.

ER Study—Al_2O_3 Replaced by AlH. The formation process of AlH discussed in Smith et al.[9] shows that AlH increases flame speeds but does not explain the reaction mechanism responsible for increased reactivity. Recall that AlH is a salt with aluminum hexahydrate $[Al(H_2O)_6]^{3+}$ interacting with the IO_3^- framework through hydrogen-bonding interactions of the coordinating water molecules. The pH-dependent process that leads to the formation of $[Al(H_2O)_6]^{3+}$ uses oxygen from Al_2O_3 to form water and Al^{3+}. Since Al^{3+} is oxidized and not expected to release energy (during the formation of Al_2O_3), the observed increase in flame speed is unexpected, and another mechanism is responsible for increased flame speeds. At this point we hypothesize that under the highly acidic (pH < 1) synthetic conditions, the Al_2O_3 passivation layer is being removed and replaced with AlH. To test this hypothesis the following figure (Figure 6) and analysis were used.

By calculating the moles of Al in 100 g of the initial mixture and the moles of Al in final AlH products using eqs 3−4a−4c, we can estimate the amount of AlH formed given the amount of Al available in Al_2O_3.

$$\mathrm{Mol}_i = \frac{\mathrm{wt}\%_i}{\mathrm{MW}_i} * 100\ \mathrm{g} \tag{3}$$

DOI: 10.1021/acs.jpcc.7b05803
J. Phys. Chem. C XXXX, XXX, XXX−XXX

Table 2. Final Concentration Data Obtained from XRD Measurements with Standard Deviation in Parentheses

ER	AlH (%)	Al^0 (%)	HI_3O_8 (%)	β-HIO_3 (%)	amorphous (%)
1.5	10.5% (2.0)	16.3% (2.8)	0%	0%	73% (3.1)
1.2	72.7% (5.2)	22.8% (1.6)	4.0% (0.5)	0.5% (0.1)	0%
1.1	76.1% (4.3)	20.0% (1.1)	3.0% (0.4)	0.9% (0.1)	0%
1	77.9% (4.7)	18.8% (1.1)	1.3% (0.2)	2.1% (0.2)	0%
0.9	57.8% (3.4)	18.6% (1.1)	11.6% (0.7)	11.9% (0.7)	0%
0.8	53.2% (2.1)	16.6% (0.7)	1.9% (0.2)	28.4% (1.1)	0%

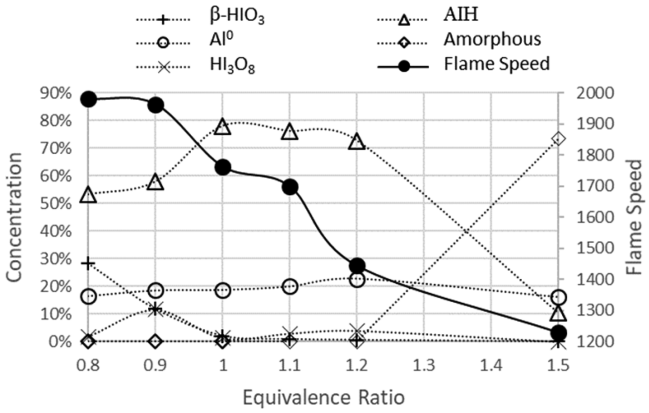

Figure 2. Flame speeds (●), AlH (Δ), aluminum (○), HIO_3 (+), HI_3O_8 (×), and amorphous (◊) concentrations as a function of ER. In all figures, dashed lines indicate concentration (wt %) and the solid line indicates flame speeds (m/s).

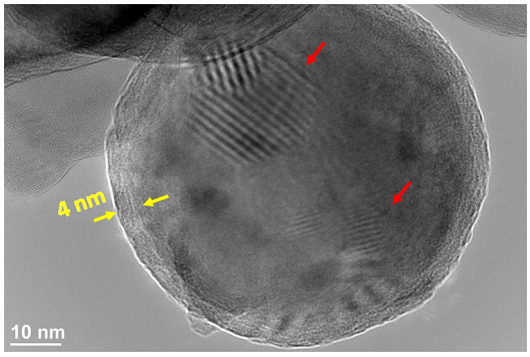

Figure 3. TEM image of Al_2O_3 passivated Al nanoparticle at 250k× magnification. The high crystallinity of the Al core is exhibited by distinct lattice fringes as indicated with red arrows. The thickness of amorphous oxide layer is measured as approximately 4 nm.

The subscript *i* in eq 3 represents the species that contain Al (i.e., Al_2O_3, AlH, and Al^0 from the core of the particle), Mol_i is moles of each species, wt % is the weight percent (shown in Tables 1 and 2) from initial mixing (subscript initial) or concentration data obtained from XRD measurement (subscript final), and MW is molecular weight. In eq 3, Mol_i represents the moles of species in initial and final mixtures (i.e., Al_2O_3, AlH, and Al^0 from the core of the particle). From the number of molecules in each mixture, the number of atoms (i.e., Al, iodine(I), and oxygen (O)) can be calculated by adding the number of atoms in each molecule. The calculation of the number of atoms used to show AlH replacement of the Al_2O_3 shell in Figure 6 is shown in eqs 4a–4c. The total initial Al ($Al_{tot,initial}$) including Al from Al_2O_3 (black line in Figure 6) is calculated using eq 4a, the final Al from only the core (Al^0) of the Al particles (Al_{core} not including Al from Al_2O_3; gray line in

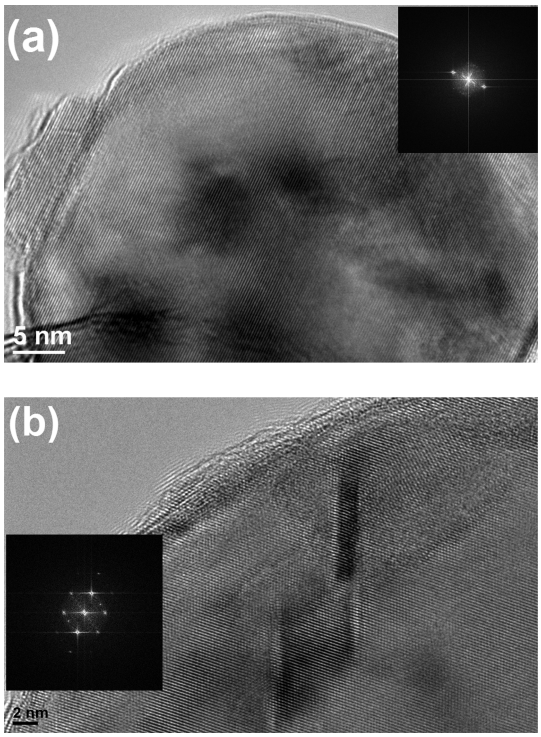

Figure 4. TEM image of Al–AlH nanoparticles: (a) at 500k× magnification and (b) at 600 k× magnification. The particles display superior single crystallinity from the Al core to the outer AlH shell exemplified by the parallel thin straight lines corresponding to lattice spacing. The inset shows the corresponding FFT plots in which a straight line drawn from a set of diffraction pair is perpendicular to the respective set of lattice fringes.

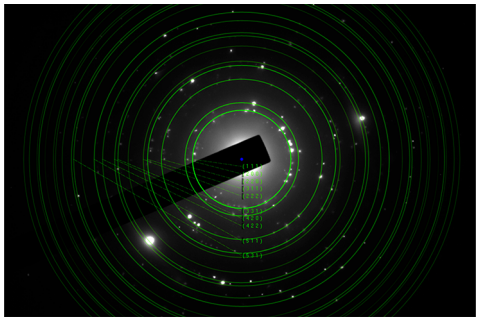

Figure 5. SAD pattern acquired from Al–AlH nanoparticles. The green circles highlight the diffraction rings of a bulk Al crystal with each ring specified by its (*hkl*) Miller index.

Figure 6) is calculated using eq 4b; the Al from final mixtures ($Al_{AlH,final}$, dashed line in Figure 6) including Al from AlH is calculated using eq 4c.

$$Al_{tot,initial} = Mol_{Al,initial} + 2*Mol_{Al_2O_3,initial} \quad (4a)$$

DOI: 10.1021/acs.jpcc.7b05803
J. Phys. Chem. C XXXX, XXX, XXX–XXX

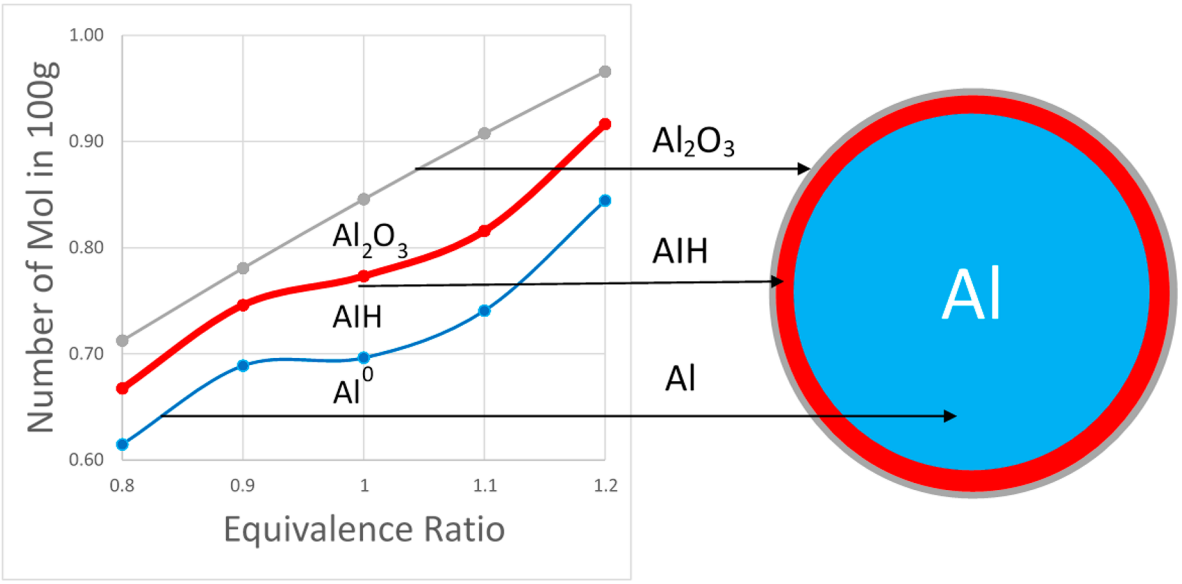

Figure 6. Schematic diagram illustrating AlH replacement of Al_2O_3 passivation layer. All lines represent the moles of Al in 100 g of initial mixture. Gray line is the moles of Al in final AlH products; blue line is the moles of Al^0 in final mixtures not including Al from Al_2O_3; red line is the number of moles of Al in final AlH products not including Al_2O_3. ER of 1.5 is not included in this graph due to large amounts of amorphous material.

$$Al_{core,final} = Mol_{Al,final} \quad (4b)$$

$$Al_{AlH,final} = Mol_{Al,final} + Mol_{AlH,final} \quad (4c)$$

Figure 6 shows that $Al_{AlH,final}$ is between $Al_{tot,initial}$ and $Al_{core,final}$ indicating that AlH forms from Al in the Al_2O_3 passivation layer and that AlH replaces the Al_2O_3 passivation layer. The initial total Al is used to show the upper limit, and the final core Al^0 is used to show the lower limit since the Al_2O_3 passivation layer is amorphous and cannot be detected by XRD measurements. However, the initial Al particles have an average diameter of 80 nm with an Al_2O_3 passivation shell that is 4 nm thick (as shown in Figure 3).[15] If it is assumed that no Al leaves as vapor during synthesis, the difference between $Al_{AlH,final}$ and $Al_{core,final}$ is the amount of AlH formed during synthesis, and the amount of final Al_2O_3 is the difference between the $Al_{tot,initial}$ and $Al_{AlH,final}$ in Figure 6.

Replacement of Al_2O_3 with AlH increases reactivity of the composite material by replacing an inert oxidation barrier (i.e., Al_2O_3) with an energetic salt (AlH), thereby increasing the amount of oxygen that can react with elemental Al^0 (Al_{core}) and decreasing the distance between Al^0 and oxygen. In nanoparticle Al oxidation reactions with an Al_2O_3 passivation layer, the oxidation of Al_{core} starts at the melting temperature of Al (approximately 660 °C depending on particle size). Volumetric expansion from molten Al allows oxygen to diffuse through the Al_2O_3 passivation layer, oxidizing molten Al from the core of Al nanoparticles.[16] In this way, Al_2O_3 acts as a diffusion barrier limiting the amount of oxygen that can react with Al from the core of the particle. Also, when the temperature of Al particles is raised to the melting temperature of Al metal, heat is absorbed by the Al_2O_3 passivation layer, a natural heat sink. By creating oxygen diffusion limitations and absorbing heat, the Al_2O_3 passivation layer raises the apparent activation energy of the system and lowers the total energy generated by Al^0 oxidation reactions.

In AlH, Al^{3+} and IO_3^- are separated by a water ring in aluminum hexahydrate, $[Al(H_2O)_6]^{3+}$. Al^{3+} in AlH has vacant 3s and 3p orbitals that allow Al^{3+} to act as a Lewis acid. When the AlH compound is heated to 135 °C, the water molecules are driven off,[17] allowing acidic Al^{3+} to react exothermically with iodate species in AlH to form Al_2O_3 and I_2 gas. The lower onset temperature (135 °C) and exothermic Al^{3+} reaction in AlH significantly lower the apparent activation energy resulting in faster reaction rates and greater total energy generated when compared to Al^0 reactions involving the Al_2O_3 passivation layer. Reaction rates are also affected by the large concentration of oxygen from AlH reactions and reduced distance between oxygen and Al^0. Since AlH replaces the Al_2O_3 shell, the spacing between Al^0 in the core and oxygen is reduced when compared to Al reactive mixtures with the Al_2O_3 passivation layer. The reaction to form Al_2O_3 from AlH is overoxidized (12.5 extra moles of oxygen for every mole of AlH). The abundance of oxygen and small spacing between available oxygen from the AlH reaction and unoxidized Al (Al^0) can significantly increase reaction rates. The combination of decreases in apparent activation energy, reduced limitations from the Al_2O_3 diffusion barrier, and shortened distance between Al^0 and oxygen from AlH reactions all account for the significant reactivity increases seen in AlH mixtures.

Significant differences in reaction behavior have also been observed in AlH mixtures that are related to concentrations of AlH, Al^0, iodic acids, and overall densities of the mixtures. In Smith et al.,[9] flame speeds increased from 1757 to 3132 m/s for AlH mixtures at a fixed ER of 1.1 when the initial water to Al ratio varied from 2:1 to 6:1. It was suggested that the dramatic increase in observed reactivity by increasing the initial water to Al ratio was caused by concentration differences or differences in density of the final material. In Smith et al.,[9] it was assumed that concentrations of AlH and Al^0 were the same for the different water to Al ratios. This assumption was necessary because β-HIO_3 had not been indexed causing high uncertainties in the quantitative analysis of the XRD measurements. Figure 7a shows the average concentration data (with uncertainties) for all samples (i.e., 2:1, 4:1, 5:1, and 6:1 water to Al ratio) with an ER of 1.1, and Figure 7b shows corresponding flame speeds for the same mixtures as a function of varying

DOI: 10.1021/acs.jpcc.7b05803
J. Phys. Chem. C XXXX, XXX, XXX−XXX

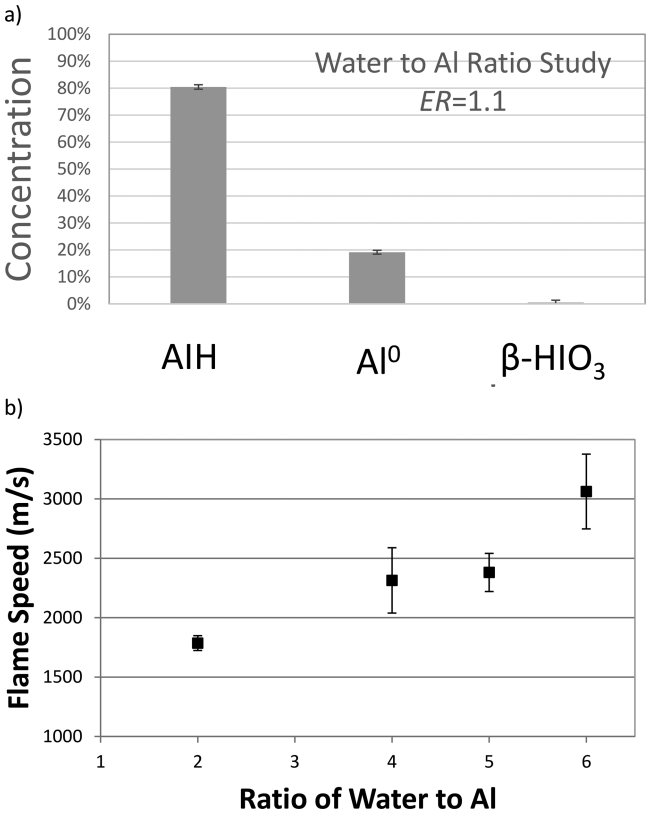

Figure 7. (a) Average concentration data for AlH, Al^0, and β-HIO_3 for fixed ER = 1.1 but for all water to aluminum ratios (i.e., 2:1, 4:1, 5:1, and 6:1 water to Al ratio). Error bars are the standard deviations in four samples. Data shows concentrations do not change as a function of the water to Al ratio. (b) Flame speed as a function of initial water to Al ratio. All samples were mixed at an initial ER of 1.1.

water concentrations. The small error bars in Figure 7a confirm that the concentration of AlH, Al, and β-HIO_3 are statistically the same in all samples with an ER = 1.1. Figure 7b shows increases in flame speed as water to Al ratio increases are not caused by differences in concentration but instead assumed to be a result of differences in density of the final material.

Examination of Figures 2 and 6 and 7does not lead to a conclusive relationship between flame speed and AlH concentration. Figure 8 shows the measured flame speed as a function of ER, oxygen balance, and concentrations of AlH, Al^0, and iodic acids. There are three clear trends shown in Figure 8a and b:

- AlH concentration significantly decreases at an ER of 0.9 compared to an ER of 1.0 (Figure 8a).
- There is a linear relation between OB and flame speed (Figure 8b).
- HIO_3 concentration increases at an ER of 0.9 and 0.8 (Figure 8c).

Figure 8a shows flame speed, oxygen balance, and AlH concentration as a function of ER (between an ER of 0.8 and 1.5). The oxygen concentrations of AlH, Al^0, and iodic acid are all accounted for when calculating OB, and in general, there is a parabolic relationship between OB and flame speed.[18] Figure 8b shows an almost linear relation between OB and flame speed (R^2 = 0.92) for a range of ER. Figure 8c shows flame speed, OB, AlH, HIO_3, and HI_3O_8 concentration as a function of ER between an ER of 0.8 and 1.1. Figures 8a and 8c show that the concentration of AlH is less at an ER of 0.8 and 0.9 when compared to concentrations of AlH at an ER of 1.0, 1.1, and 1.2. The HIO_3 and HI_3O_8 concentration increases rapidly (Figure 8c) at an ER of 0.8 and 0.9 compared to ER of 1.0, 1.1, and 1.2. The ER range in Figure 8c is reduced because of the amorphous structure beginning at an ER of 1.5 (see Figure 2). The composition of the amorphous structure cannot be determined; thus, accurate fuel to oxygen ratios (OB) cannot be calculated, and OB for an ER of 1.5 is an estimate.

The linear relation between OB and flame speed (Figure 8b) is unexpected because there is normally a parabolic trend between OB and reactivity with the greatest reactivity seen with a slightly fuel rich mixture. With the assumption that the greatest reactivity will be seen where OB is slightly fuel rich (ER = 1.0), it is unexpected to see increased reactivity at an ER of 0.8 and 0.9 compared to ER of 1.0. The increase in flame speed corresponds with decreased AlH concentrations (below ER = 1.0) and decreased Al_2O_3 concentrations (Figure 8). Figure 8 shows Al_2O_3 concentration in the final AlH mixtures determined by the distance between dashed line and solid black line. The concentration of Al_2O_3 is greater at an ER of 1.0 compared to an ER of 0.9 and can account for the increase in flame speed at ER = 0.9. Smith et al.[19] (see Figure 3 from ref 19.) show that all the initial Al_2O_3 reacts with the acidic solution but only a portion forms AlH. The Al_2O_3 that forms as a byproduct of AlH formation may not be a uniform layer and may be less of a diffusion barrier than the original Al_2O_3 layer. In this way, Al_2O_3 that forms as a byproduct of AlH formation will act mainly as a heat sink and not a diffusion barrier. Another factor that influences the difference in flame speed between an ER of 0.9 and 1.0 is the amount of Al^0. Al^0 is a fuel for AlH reactions, and reducing the amount of Al^0 will reduce the amount of total energy generation. Concentrations of iodic acids, β-HIO_3 at an ER of 0.8 and both β-HIO_3 and HI_3O_8 at an ER of 0.9, are highest when flame speeds are highest. All of these aspects, OB, concentration of AlH, Al_2O_3, Al^0, and iodic acids, need to be considered when examining concentration effects on flame speed. Because there is no direct relation between flame speed and concentration of AlH or Al_2O_3, we propose that, in general, reactivity is directly related to relative concentration of AlH and Al_2O_3, shown in Table 3 as AlH to Al_2O_3 ratio. Table 3 shows that, in general, higher AlH/Al_2O_3 ratios have faster flame speeds when OB is considered. In Table 3, there is a linear relation between AlH to Al_2O_3 ratio and flame speed between an ER of 1.1 and 0.9. At an ER of 1.2, AlH to Al_2O_3 ratio increases but flame speed significantly decreases; however, OB also decreases significantly. The decrease in flame speed between an ER of 1.1 and 1.2 that does not follow the AlH to Al_2O_3 ratios relation to flame speed can be explained by the significant decrease in OB. At an ER of 0.8, flame speeds continue to increase, but AlH to Al_2O_3 ratio decreases and OB increases. We propose that the increase in flame speed between an ER of 0.9 and 0.8 is a result of increased concentrations of iodic acids, specifically, β-HIO_3. The reason why β-HIO_3 increases flame speed is unknown and requires further study.

It is interesting to note that β-HIO_3 is stable in AlH mixtures. Smith et al. show that β-HIO_3 is metastable when aged for a period of 8 days after being ground for powder XRD measurements. The AlH samples shown here were aged after being ground for a period of months, and β-HIO_3 did not convert into α-HIO_3, indicating that AlH stabilizes β-HIO_3.

DOI: 10.1021/acs.jpcc.7b05803
J. Phys. Chem. C XXXX, XXX, XXX−XXX

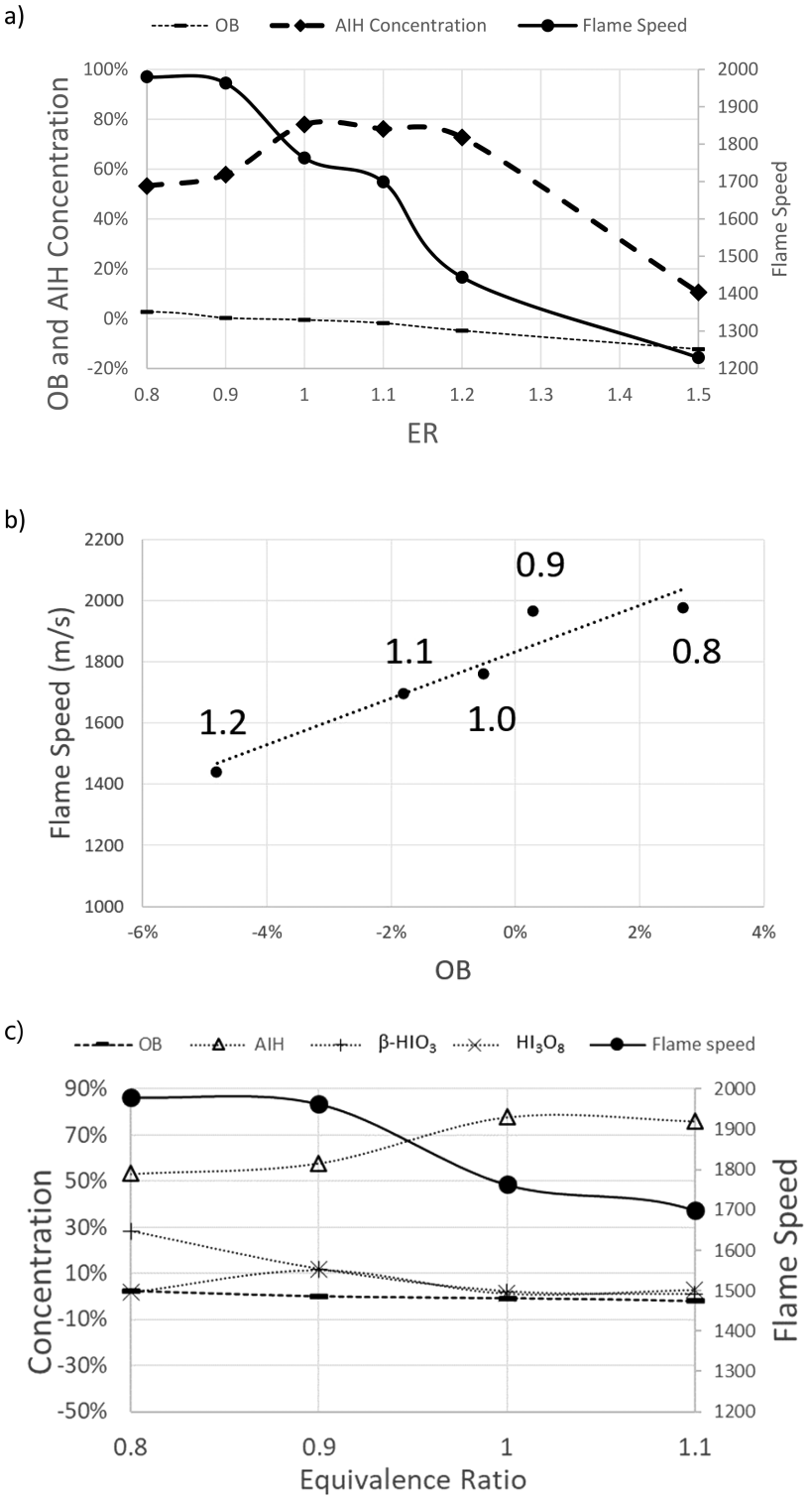

Figure 8. (a) Flame speeds (●), OB (−), and AlH concentration (Δ) as a function of ER. (b) Flame speed as a function of OB. Dashed line is a linear fit with R^2 value of 0.92. (c) Zoom-in of Figure 8a between ER of 0.8 and 1.1 with HIO_3 (+) and HI_3O_8 (□).

CONCLUSIONS

AlH increases reactivity in Al energetic materials by replacing the Al_2O_3 passivation layer that naturally forms on Al particles with AlH. The Al_2O_3 acts as a heat sink and oxygen diffusion barrier, and replacement of the Al_2O_3 passivation layer with AlH significantly reduces the diffusion barrier and facilitates Al^0 oxidation. The Al−AlH single-crystalline structure without the amorphous Al_2O_3 layer was carefully assessed and examined under TEM. The images revealed distinct single crystalline lattice fringes throughout the entire particle from the Al core to the outer AlH shell with perfect conformity. Also, FFT plots confirm the crystallinity, and the SAD pattern confirms that distinct diffraction spots have lattice spacing consistent with those of a bulk Al crystal. The reaction to form Al_2O_3 from AlH is extremely overoxidized (i.e., 12.5 mol of extra oxygen for every mole of AlH), and replacement of the Al_2O_3 passivation

DOI: 10.1021/acs.jpcc.7b05803
J. Phys. Chem. C XXXX, XXX, XXX−XXX

Table 3. Factors That Influence Flame Speed

ER	AlH/Al_2O_3	OB	β-HIO_3 (wt %)	HI_3O_8 (wt %)	flame speed (m/s)
1.2	2.90	−4.8%	0.6%	4.0%	1444
1.1	1.64	−1.8%	0.9%	3.0%	1699
1	2.13	−0.5%	2.1%	1.3%	1736
0.9	3.29	0.3%	11.9%	11.6%	1863
0.8	2.33	2.7%	28.4%	1.9%	1980

layer with AlH increases the available oxygen and reduces the distance between unreacted Al in the core and oxidizer. The combined effects of reducing the diffusion barrier and reduced distance between fuel and oxidizer result in flame speeds as high as 3200 m/s in Al−AlH mixtures.

Flame speed is affected by the concentrations of AlH, Al^0, Al_2O_3, and iodic acids of Al−AlH mixtures. In general, higher ratios of AlH to Al_2O_3 increase flame speeds. Since oxygen is supplied by iodic acids in AlH mixtures, the effects of iodic acids on flame speed can be summarized by oxygen balance. Decreases in flame speed are seen when the AlH to Al_2O_3 ratio is relatively high and oxygen balance is significantly away from stoichiometric. An increase in reactivity is seen when oxygen balance is 2.6% and AlH to Al_2O_3 ratio is less than 2.0 at an ER of 0.8. At an ER of 0.8, β-HIO_3 concentration is the highest reported, and the increase in reactivity at ER 0.8 could be a result higher concentrations of β-HIO_3.

AUTHOR INFORMATION

Corresponding Author

*Phone: 806-834-3733. E-mail: michelle.pantoya@ttu.edu.

ORCID

Michelle L. Pantoya: 0000-0003-0299-1832

Notes

The authors declare no competing financial interest.

ACKNOWLEDGMENTS

The authors are grateful for support from the Army Research Office under award W911NF-14-1-0250 and encouragement from our program manager, Dr. Ralph Anthenien. We are also grateful to Dr. Jennifer Gottfried from ARL for constructive feedback on this work.

REFERENCES

(1) Kappagantula, K. S.; Pantoya, M. L. Fast-Reacting Nanocomposite Energetic Materials: Synthesis and Combustion Characterization. In *Energetic Nanomaterials Synthesis, Characterization and Apllication*; Zarko, V. E., Gromov, A. A., Eds.; Elsevier: Cambridge, MA, 2016; pp 21−45.

(2) Weinheimer, R. Properties of Selected High Explosives. *Proc. 27th Int. Pyrotech. Semin.* **2000**, 1−37.

(3) Fischer, S. H.; Grubelich, M. C. Theoretical Energy Release of Thermites, Intermetallics and Combustible Metals. *Semin. Int. Pyrotech.* **1998**, 10.2172/658208.

(4) Mulamba, O.; Pantoya, M. Exothermic Surface Reactions in Alumina−Aluminum Shell−Core Nanoparticles with Iodine Oxide Decomposition Fragments. *J. Nanopart. Res.* **2014**, *16* (3), 2310.

(5) Bockmon, B. S.; Pantoya, M. L.; Son, S. F.; Asay, B. W.; Mang, J. T. Combustion Velocities and Propagation Mechanisms of Metastable Intermolecular Composites. *J. Appl. Phys.* **2005**, *98* (6), 64903.

(6) Brousseau, P.; Dorsett, H.; Cliff, M.; Anderson, C. Detonation Properties of Explosives Containing Nanometric Aluminum Powder. *12th Int. Detonation Symp.* **2002**, 1−10.

(7) Padhye, R.; McCollum, J.; Korzeniewski, C.; Pantoya, M. L. Examining Hydroxyl-Alumina Bonding toward Aluminum Nanoparticle Reactivity. *J. Phys. Chem. C* **2015**, *119* (47), 26547−26553.

(8) Smith, D. K.; McCollum, J.; Pantoya, M. L. Effect of Environment of Iodine Oxidation State on Reactivity with Aluminum. *Phys. Chem. Chem. Phys.* **2016**, *18*, 11243−11250.

(9) Smith, D. K.; Bello, M. N.; Unruh, D. K.; Pantoya, M. L. Synthesis and Reactive Characterization of Aluminum Iodate Hexahydrate Crystals $[Al(H_2O)_6](IO_3)_3(HIO_3)_2$. *Combust. Flame* **2017**, *179*, 154−156.

(10) Rinaldi, R.; Fujiwara, F. Y.; Schuchardt, U. Hexaaquoaluminum-(III) as an Environmental Friendly Activator of Hydrogen Peroxide for the Catalytic Epoxidation of Cis-Cyclooctene. *Catal. Commun.* **2004**, *5* (6), 333−337.

(11) Little, B. K.; Emery, S. B.; Nittinger, J. C.; Fantasia, R. C.; Lindsay, C. M. Physiochemical Characterization of Iodine (V) Oxide, Part 1: Hydration Rates. *Propellants, Explos., Pyrotech.* **2015**, *40*, 595−603.

(12) Kumar, R.; Saunders, R. W.; Mahajan, a. S.; Plane, J. M. C.; Murray, B. J. Physical Properties of Iodate Solutions and the Deliquescence of Crystalline I_2O_5 and HIO_3. *Atmos. Chem. Phys.* **2010**, *10* (24), 12251−12260.

(13) Ayache, J.; Beaunier, L.; Boumendil, J.; Ehret; Gabrielle, E.; Laub, D. *Sample Preparation Handbook for Transmission Electron Microscopy Techniques*; Springer: New York, 2009.

(14) Smith, D. K.; Unruh, D. K.; Pantoya, M. L. Re-Discovery of β-HIO_3: A Metastable Polymorph of HIO_3. Under review, 2017.

(15) Gesner, J.; Pantoya, M. L.; Levitas, V. I. Effect of Oxide Shell Growth on Nano-Aluminum Thermite Propagation Rates. Combust. *Combust. Flame* **2012**, *159* (11), 3448−3453.

(16) Levitas, V. I.; Asay, B. W.; Son, S. F.; Pantoya, M. Melt Dispersion Mechanism for Fast Reaction of Nanothermites. *Appl. Phys. Lett.* **2006**, *89* (7), 071909.

(17) Cradwick, P. D.; Endredy, A. S. d. Crystal Structre of Aluminium Iodate−Hydrogen Iodate−Water (1/1/6) and Preparation of Anhydrous Aluminium Iodate. *J. Chem. Soc., Dalton Trans.* **1977**, *2*, 146−149.

(18) Mendoza Orbegoso, E. M.; Silva, L. F. F. da.; Novgorodcev Junior, A. R. On the Predictability of Chemical Kinetics for the Description of the Combustion of Simple Fuels. *J. Brazilian Soc. Mech. Sci. Eng.* **2011**, *33* (4), 492−505.

(19) Smith, D. K.; Unruh, D. K.; Pantoya, M. L. Replacing the Al_2O_3 Shell on Al Particles with an Energetic Salt, Aluminum Iodate Hexahydrate. Part II: Synthesis. *J. Phys. Chem. C* **2017**, DOI: 10.1021/acs.jpcc.7b05805.

DOI: 10.1021/acs.jpcc.7b05803
J. Phys. Chem. C XXXX, XXX, XXX−XXX